

THE JET OF 3C 17 AND THE USE OF JET CURVATURE AS A DIAGNOSTIC OF THE X-RAY EMISSION PROCESS

F. MASSARO¹, D. E. HARRIS¹, M. CHIABERGE^{2,7}, P. GRANDI³, F. D. MACCHETTO², S. A. BAUM⁴, C. P. O'DEA⁵ AND A. CAPETTI⁶

version 2009 Jan 26: fm/deh

ABSTRACT

We report on the X-ray emission from the radio jet of 3C 17 from *Chandra* observations and compare the X-ray emission with radio maps from the VLA archive and with the optical-IR archival images from the Hubble Space Telescope. X-ray detections of two knots in the 3C 17 jet are found and both of these features have optical counterparts. We derive the spectral energy distribution for the knots in the jet and give source parameters required for the various X-ray emission models, finding that both IC/CMB and synchrotron are viable to explain the high energy emission. A curious optical feature (with no radio or X-ray counterparts) possibly associated with the 3C 17 jet is described. We also discuss the use of curved jets for the problem of identifying inverse Compton X-ray emission via scattering on CMB photons.

Subject headings: Galaxies: active — galaxies: jets — galaxies: individual (3C 17) — X-rays: general — radio continuum: galaxies — radiation mechanisms: nonthermal

1. INTRODUCTION

The X-ray radiation observed from radio jets is generally interpreted to be from non-thermal processes, even if its nature is still unclear for any particular jet. It could be described in terms of synchrotron emission or in terms of several varieties of inverse Compton radiation. So to understand the emission mechanisms related to these components the multiwavelength approach is required. If the X-ray emission is synchrotron, electrons with Lorentz factors γ up to 10^7 are required whereas if the process is inverse Compton radiation with seed photons due to the CMB (Tavecchio et al., 2000), the X-rays would come from electrons with $\gamma \approx 100$ (Harris & Krawczynski 2002). To investigate the nature of the emission in jets we analyze the jet of the powerful radio galaxy 3C 17.

3C 17 was observed during the first year of the *Chandra* 3C snapshot program, which started in AO-9 with 8ks observations of 30 of the previously unobserved (by *Chandra*) 3C sources with $z < 0.3$. The 3C sample allows us to have multifrequency data available from the HST and the VLA archives. 3C 17 is a radio galaxy ($z \sim 0.22$, Schmidt et al. 1965) with a peculiar radio structure investigated by Morganti et al. (1999). Its H α emission has a strong broad component and both the [O II] $\lambda 3727$ and [O III] $\lambda 5007$ emission lines are extended (Dickson

1997). This source shows also a significant optical polarization in its nucleus (Tadhunter et al. 1998), and its first detection in X-rays has been reported by Siebert et al. (1996) using the ROSAT All Sky survey data.

Here, we report the major results concerning the multiwavelength studies of the jet in 3C 17. We present the X-ray data of this source together with the optical-IR images (HST) and the radio maps (VLA archive).

For our numerical results, we use cgs units unless stated otherwise and we assume a flat cosmology with $H_0 = 72 \text{ km s}^{-1} \text{ Mpc}^{-1}$, $\Omega_M = 0.27$ and $\Omega_\Lambda = 0.73$ (Spergel et al., 2007), so $1''$ is equivalent to 3.47 kpc. Spectral indices, α , are defined by flux density, $S_\nu \propto \nu^{-\alpha}$.

2. OBSERVATIONS AND DATA REDUCTION

2.1. X-rays data

3C 17 has been observed by *Chandra* (Obs ID 9292) on February 2, 2008, with the ACIS-S camera, operating in VFaint mode, with an exposure of about 8 ksecs. The data reduction has been performed following the standard procedures described in the *Chandra* Interactive Analysis of Observations (CIAO) threads and using the CIAO software package v3.4. The *Chandra* Calibration Database (CALDB) version 3.4.2 was used to process all files. Level 2 event files were generated using the *acis_process_events* task, after removing the hot pixels with *acis_run_hotpix*. Events were filtered for grades 0,2,3,4,6 and we removed pixel randomization. Astrometric registration was done changing the appropriate keywords in the fits header so as to align the nuclear X-ray position with that of the radio. We also registered the HST images in the same way.

We created 3 different fluxmaps (soft, medium, hard, in the ranges 0.5 – 1, 1 – 2, 2 – 7 keV, respectively) by dividing the data with the exposure maps. When constructing the fluxmaps, we normalized each count by multiplying by $h\nu$ where ν corresponds to the energy used for the corresponding exposure map. Thus we can measure the flux in any aperture in cgs units with only a

¹ Harvard, Smithsonian Astrophysical Observatory, 60 Garden Street, Cambridge, MA 02138

² Space Telescope Science Institute, 3700 San Martine Drive, Baltimore, MD 21218

³ Carlson Center for Imaging Science 76-3144, 84 Lomb Memorial Dr., Rochester, NY 14623

⁴ INAF-IASF - Istituto di Astrofisica Spaziale e fisica cosmica di Bologna, Via P. Gobetti 101, 40129, Bologna, Italy

⁵ Dept of Physics, Rochester Institute of Technology, Carlson Center for Imaging Science 76-3144, 84 Lomb Memorial Dr., Rochester, NY 14623

⁶ INAF - Osservatorio Astronomico di Torino, Strada Osservatorio 20, I-10025 Pino Torinese, Italy

⁷ INAF - Istituto di Radioastronomia di Bologna, via Gobetti 101 40129 Bologna, Italy

small correction for the ratio of the mean energy of the counts within the aperture to the nominal energy for the band.

Photometric apertures were constructed so as to accommodate the Chandra point spread function and so as to include the total extent of the radio structure. They are shown in fig. 1. The background regions have been chosen close to the source with comparable size, typically two times bigger than the source region, centered on a position where other sources or extended structure are not present. All X-ray flux densities have been corrected for the Galactic absorption with the N_H column densities given by Kalberla et al. (2005), $2.86 \cdot 10^{20} \text{cm}^{-2}$.

2.2. Radio maps and HST images

We compare our X-rays maps of 3C 17 with the VLA radio data described in Morganti et al. (1999) at 4.8 GHz with a beamsize of $0.4''$. We also reduced archival VLA data at 1.54 GHz and 14.9 GHz with AIPS standard reduction procedures. The angular resolution of these radio maps is $\approx 1.4''$ and the final image is in good agreement with the 4.8 GHz radio map. The amplitude calibrator used at 1.4 GHz was 3C 48 and the phase calibrator was 0056-001. At 15GHz we used 0106+103 for both amplitude and phase.

Concerning the other bands, we compared our X-ray image to the IR HST observation at $1.6 \mu\text{m}$ ($1.87 \cdot 10^{14}$ Hz, H band)⁸, and to the STIS visible image at $4.16 \cdot 10^{14}$ Hz (7216 \AA , R band). We also used a FUV HST image at 1457 \AA .

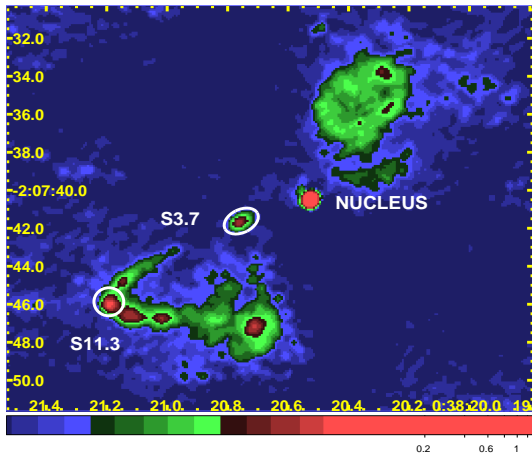


FIG. 1.— The 5 GHz VLA map of Morganti et al. (1999) with a restoring beam of $0.4''$. The two knots of interest are emphasized (in white) with the regions used for photometry.

3. RESULTS

3C 17 is a broad lined radio galaxy (BLRG) (Buttiglione et al. 2008) with a monochromatic radio luminosity, $\log P_{1.4\text{GHz}} \approx 26.9$ which is at least two orders of magnitude above the division between FRI and FRII types (Ledlow & Owen, 1996) but with an ambiguous radio morphology. Miller & Brandt (2008) provide a more extensive discussion on classifying sources of this

⁸ available on the *HST Snapshots of 3CR Radio Galaxies* webpage, <http://archive.stsci.edu/prepds/3cr/>

TABLE 1
OBSERVED X-RAY COUNTS AND FLUXES FOR JET FEATURES.

	Soft	Medium	Hard	Total
Nominal Energy (keV)	0.70	1.4	4.0	
Band (keV)	0.5-1.0	1-2	2-7	0.2-7
S3.7 counts	5	6	1	12
S11.3 counts	1	0	4	5
S3.7 flux	2.6 ± 1.1	2.2 ± 0.9	1.6 ± 1.6	6.4
S11.3 flux	0.6 ± 0.5	0	6.5 ± 3.3	7.1

Flux units: $10^{-15} \text{ erg cm}^{-2} \text{ s}^{-1}$.

Notes to table:

The average backgrounds measured for the total 0.5-7 keV band from annular rings around the radio galaxy are 1.57 counts (S3.7) and 0.08 counts (S11.3).

'hybrid' type, including 4C65.15, which is very similar to 3C 17 in many respects.

The nucleus of the host galaxy has been observed with the Very Long Baseline Array by Venturi et al. (2000) who describe 3C 17 as a "transition object" between FRI and FRII. The pc scale jet shows a 'core' with an extension in $\text{PA} \approx 100^\circ$ to 110° , followed by lower brightness features. This position angle is essentially the same as that of the first kpc scale knot, S3.7, discussed below.

The kpc scale radio morphology is dominated by a single sided, strongly curved jet (fig. 1, as described by Morganti et al. 1993, 1999), although there is lower brightness emission outside the area covered in the figure. Similarly to M87, 3C 17 was originally classified as a 'core-halo' source. The jet has a bright knot at $3.7''$ from the nucleus while the curved part lies at about $11''$ from the nucleus.

3.1. Jet knots

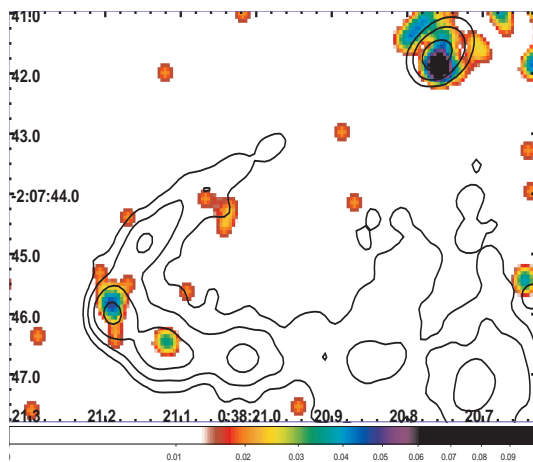


FIG. 2.— The Chandra X-ray map. Pixel randomization has been removed and the events between 0.5 and 7 keV were smoothed with a Gaussian of $\text{FWHM} = 0.87''$. The radio contours come from fig. 1 and start at 0.5 mJy/beam, increasing by factors of 4. S3.7 is at the upper right and S11.3 to the lower left.

Using our new Chandra observation we find detections of two knots (fig. 2). The first knot, S3.7, lies at a projected distance of 12.8 kpc from the nucleus and is resolved with the VLA. The deconvolved size (FWHM) is $0.46'' \times 0.18''$ (1.6×0.6 kpc) in $\text{PA} = 115^\circ$. Following a

TABLE 2
FLUX DENSITIES (CGS UNITS) FOR 3C 17 KNOTS

Freq. (Hz)	Band	S3.7	S11.3
$1.66 \cdot 10^9$	L	$80 \pm 10 \cdot 10^{-26}$	$(190 \pm 10 \cdot 10^{-26})$
$4.86 \cdot 10^9$	C	$30 \pm 1 \cdot 10^{-26}$	$83 \pm 2 \cdot 10^{-26}$
$1.49 \cdot 10^{10}$	U	$12.4 \pm 1 \cdot 10^{-26}$	$(33 \pm 10 \cdot 10^{-26})$
$1.87 \cdot 10^{14}$	$1.6 \mu\text{m}$	$3.28 \pm 0.16 \cdot 10^{-29}$...
$4.16 \cdot 10^{14}$	7216 \AA	$1.44 \pm 0.13 \cdot 10^{-29}$	$1.03 \pm 0.07 \cdot 10^{-29}$
$2.06 \cdot 10^{15}$	1457 \AA	$0.15 \pm 0.03 \cdot 10^{-29}$	$0.054 \pm 0.018 \cdot 10^{-29}$
$1.18 \cdot 10^{17}$	soft X	$1.86 \pm 0.8 \cdot 10^{-32}$	$0.56 \pm 0.27 \cdot 10^{-32}$
$3.39 \cdot 10^{17}$	medium X	$1.04 \pm 0.42 \cdot 10^{-32}$	$< 0.3 \cdot 10^{-32}$
$9.67 \cdot 10^{17}$	hard X	$0.14 \pm 0.14 \cdot 10^{-32}$	$0.56 \pm 0.28 \cdot 10^{-32}$

Notes to table

Values in parentheses are uncertain because a $1.4''$ beamsize is inadequate to isolate S11.3 from adjacent knots.

gap with no detectable radio emission, the jet again becomes visible in the radio about $7''$ from the nucleus and brightens as it approaches the region of maximum apparent curvature. It is at this point we detect X-rays from the radio knot, S11.3, which has the highest radio surface brightness (after the nuclear emission). Its deconvolved radio size is $0.4'' \times 0.3''$ (1.4×1.0 kpc) in PA= 48° .

X-ray fluxes for both knots are given in Table 1 and flux densities, evaluated for a spectral index equal to 1, are listed in Table 2. The total number of counts detected for S3.7 and for S11.3 is 12 and 5 respectively, where the average background evaluated around each knot is 1.57 cts for S3.7 and 0.08 cts for S11.3 for the same size aperture.

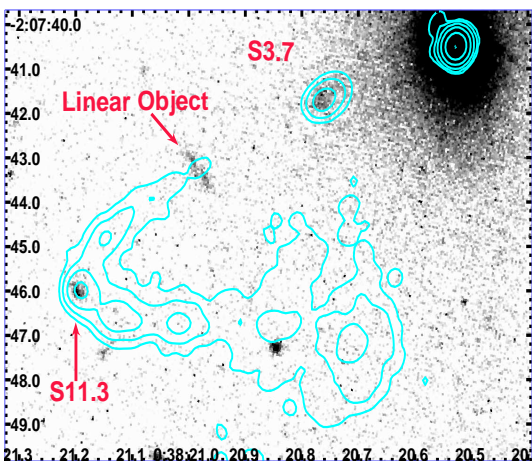


FIG. 3.— HST optical image of 3C 17 (7216 \AA). The overlaid cyan contours are the same as those in fig. 2. Here, the radio knots at $3.7''$ and $11.3''$ show optical counterparts. The linear object discussed in the text lies at about $7.4''$ from the nucleus.

We compared also the radio and the X-ray emission with the optical and IR images reported by Donzelli et al. (2007). The knot S3.7 shows a counterpart both in the optical and in the IR image. For the other knot, S11.3, we report only the optical association because the FOV of the NICMOS camera is too small. The IR to UV flux densities are corrected for the reddening using the following values of absorption: $A_H=0.01$, $A_R=0.062$ and $A_{UV}=0.044$, for the IR, the R band and the UV

respectively (Cardelli et al. 1989)⁹. The SED of each knot is shown in figs. 4 & 5.

We tried several models to fit the emitted spectrum of both knots in 3C 17. We describe the spectrum from the radio band to the UV in terms of synchrotron emission but consider both synchrotron and IC/CMB for the X-rays. We performed our calculations assuming the following hypothesis: (1) the distribution of emitting electrons is a power-law with slope s ; (2) the volumes of the emitting regions correspond to the deconvolved radio sizes; (3) the magnetic field is in equipartition with the energy density of the relativistic electrons; and (4) the proton-to-electron ratio is assumed to be zero.

Based on these assumptions, the spectrum is described in terms of 4 parameters, namely: the slope of the electron distribution s , the maximum and the minimum energy of emitting particles γ_{max} , γ_{min} and the magnetic field, because we fixed the volume derived from the radio maps.

The spectral index of the electron distribution has been derived from the observed spectrum fitting the radio to optical data with a power-law (see Tab.3). The maximum energy of particles has been evaluated in order to see the synchrotron exponential cut-off in the UV, as suggested by the data. Finally, given the value of the magnetic field and assuming a minimum observed frequency of 10^7 Hz , we derived the γ_{min} parameter for both electron distribution (see Tab. 3). Following this criteria we found that the γ_{min} is the order of 100 for both knots, it correspond to an electron minimum energy of about 50 MeV, that can be predicted by several acceleration processes (e.g. Protheroe 2004). Finally, the values of the magnetic field, reported in Tab.3, are related to the synchrotron interpretation, but are only slightly different for the smaller γ_{min} .

Solutions shown in figs. 4 & 5 have the beaming factor fixed to 1. We find a good agreement of our solution with the observed spectrum for a magnetic field of $180 \mu\text{G}$ for S3.7 and $195 \mu\text{G}$ for S11.3. Parameters for our model are reported in Table 3.

For an inverse Compton (IC) model using photons of the microwave background (CMB) we follow the formalism of Harris & Krawczynski (2002). For S3.7, we find that the required beaming factor is $\delta=8$ for the fiducial condition $\delta = \Gamma$ (Γ is the bulk Lorentz factor of the jet knot). The angle to the line of sight for this solution is $\theta=7^\circ$ although smaller angles together with smaller Γ are also acceptable. For S11.3, the values for the fiducial condition are $\delta = \Gamma=5.5$ and $\theta=10^\circ$. Since the jet is obviously curved, there is no expectation that the two values of θ should be equal even if one might guess that S11.3 would be moving more towards us than S3.7. These estimates are very rough because of the poor signal to noise in the X-ray data and because we do not have a measure of the radio spectral index.

It should be noted that the IC/CMB interpretation rests solely on the UV flux densities which are approximately 5 sigma for S3.7 and less than 3 sigma for S11.3 below the single power-law extending to the X-ray data. Because of the low statistical significance of these data and because of the added uncertainty of the extinction

⁹ see also “Doug’s Excellent Absorption Law Calculator”, <http://www.macho.mcmaster.ca/JAVA/Acurve.html>

correction, we do not rule out a synchrotron spectrum extending out to the X-rays as shown by the dotted lines in figures 4 & 5. However the low UV flux values favor the IC/CMB interpretation instead of the single synchrotron component. A more accurate observation in the UV band (down to $\sim 1200\text{\AA}$) is needed to distinguish between models, e.g. if the spectrum is curved in the IR-to-UV range then the single synchrotron component could be ruled out.

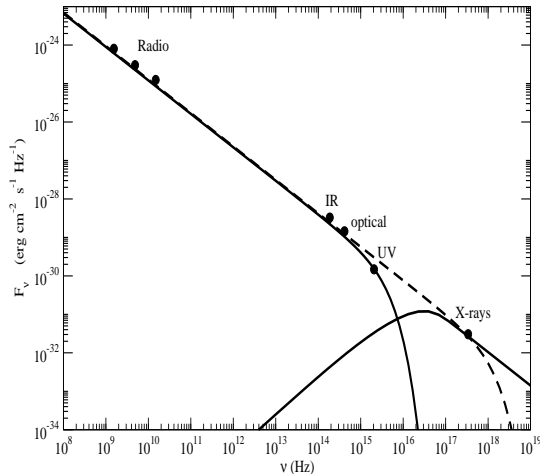


FIG. 4.— The spectrum of S3.7. The synchrotron calculations (done under the assumptions described in §3) fit the radio to UV with a cutoff, or extend to the X-ray ignoring the UV datum (dashed line). The IC/CMB model is the separate component peaking just below 10^{17}Hz .

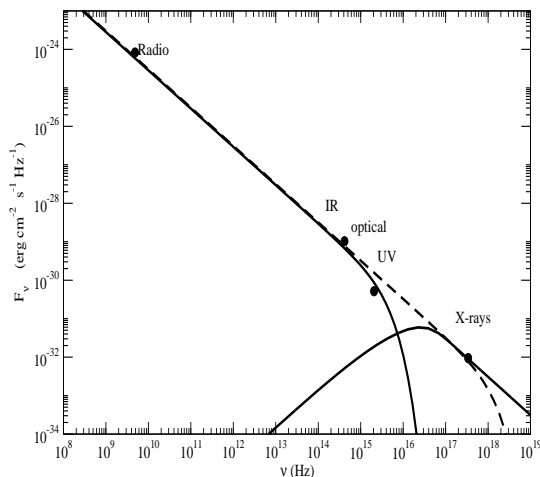


FIG. 5.— The spectrum of S11.3 See the caption of fig. 4.

TABLE 3
MODEL PARAMETERS FOR THE SYNCHROTRON CALCULATIONS.

Parameter (cgs units)	S3.7	S11.3
Spectral Index, α_{ro}	0.87	0.99
Electron index $s = 2\alpha + 1$	2.74	2.98
γ_{min}	104	100
$\gamma_{max}(\text{IC/CMB})$	$1.8 \cdot 10^6$	$2.2 \cdot 10^6$
$\gamma_{max}(\text{synchrotron})$	$3.1 \cdot 10^7$	$2.8 \cdot 10^7$
Magnetic field (10^{-6} G)	180	195
Volume (10^{64}cm^3)	1.81	4.21
Luminosity (10^{43} erg s^{-1})	1.36	0.98

Notes to table

- a) Two values of γ_{max} are listed. The IC/CMB entry is for the case where the synchrotron spectrum cuts off after the UV data whereas the synchrotron entry is for a synchrotron spectrum extending to the X-ray band.
b) The values of the magnetic field reported are related to the synchrotron interpretation.

TABLE 4
FLUX DENSITIES FOR THE LINEAR OBJECT.

Frequency	Flux density
5 GHz	< 0.5 mJy
$1.6 \mu\text{m}$	$4.8 \pm 0.3 \mu\text{Jy}$
7216\AA	$0.73 \pm 0.04 \mu\text{Jy}$
1457\AA	< 0.15 nJy
$1 \times 10^{18}\text{Hz}$	< 0.1 nJy

3.2. A peculiar optical feature

We noticed a linear optical feature on both HST images: $1.6 \mu\text{m}$ and 7216\AA (fig. 3). It is a little over an arcsec long (3.5kpc if at the distance of 3C 17), with a major axis within 11° of the perpendicular to the jet at just the point where the radio emission recommences after the 'gap' following S3.7. This feature is $\approx 7.3''$ (a projected distance of 25kpc) from the nucleus and has an optical AB magnitude of ≈ 23 . At 7200\AA , there is a 'hole' in the center; one or more pixels are comparable to the background level. At $1.6\mu\text{m}$, there is no hole. If we measure just the outer bits, we find a two-point spectral index, $\alpha_o = 1.7 \pm 0.2$. If we measure the entire object, it is 2.2 ± 0.2 . There is no evidence of X-ray or radio emission corresponding to this feature. Flux densities and upper limits are given in Table 4.

If the object were an edge on spiral at the same distance of 3C 17, its absolute magnitude would be -17 which, when coupled with an overall size of 3.5 kpc would mean it could be classified as a dwarf spiral (see Schombert et al. 1995).

We consider 4 types of possible explanations for this object.

- The object is a foreground or background object (e.g. edge on spiral) and has nothing whatsoever to do with the jet. A rough estimate of the probability of the jet crossing a random background source within the $0.2''$ nuclear region (defined by the lowered brightness center at 7216\AA) is $0.2/360 = 5 \times 10^{-4}$. However, since we don't know

how to estimate the probability that the (upstream) invisible jet just happens to start converting some of its power into relativistic electrons and B field at this location, and since we are wary of *a posteriori* probabilities, the 'chance alignment' hypothesis seems unlikely, but remains a possibility.

- The emitting region arises from the interaction of the jet and some pre-existing entity (e.g. a large HI cloud, only a part of which gets ionized and produces free-free emission). This hypothesis can be tested with an optical spectrum since the most likely method of creating optical emission from the interaction of a jet and cold gas would be via ionization leading to recombination lines and an optically thin continuum. Since the observed spectrum is inconsistent with free-free emission from an ionized gas at $> 10^4\text{K}$, it would have to be dominated by emission lines. The two observed bands correspond to 1.27-1.36 μ and 5452-6387 angstroms at the redshift of 3C 17. Neither of these bands would be expected to contain the more likely emission lines envisaged by this scenario.
- The emitting region comes from an unknown property of the jet. To our knowledge, no other jet exhibits such a narrow band feature perpendicular to its axis.
- The object is indeed an edge on spiral and is a close companion of 3C 17. The jet pierces the center of this galaxy and that is why the jet begins to be visible at this location. This jet, like all one sided jets, is coming 'mostly' towards us: perhaps $10^\circ - 30^\circ$ to the l.o.s. for this section of the jet. Since the edge on spiral's plane is perpendicular to the plane of the sky, the actual impacting jet will be close to hitting the plane of the galaxy at an oblique angle, not coming in at the pole, as it appears in the projected view. In any event the probability of hitting an object whose center subtends 1 kpc^2 (as seen from the SMBH of 3C 17) by chance is $\frac{1}{4\pi R^2} \leq 1.3 \times 10^{-4}$ (again, an *a posteriori* probability).

If we refuse to allow 'intent' (e.g. 'intergalactic engineering'), we are left with an improbable chance alignment, an interaction with some pre-existing entity, or some new type of jet-related emission. An optical spectrum of this object could eliminate some of these possibilities.

4. HOW CURVED JETS CAN PROVIDE EVIDENCE FOR IC/CMB X-RAY EMISSION

Most jets that have been well studied are relatively straight and the assumption is normally made that θ , the angle to the l.o.s., does not change along the jet. A curving jet provides an advantage because a changing viewing angle should be reflected in the run of the ratio, R, of X-ray to radio intensities differently for synchrotron and IC emissions. If, and only if, the X-ray emission is dominated by IC/CMB emission will the emitting regions closer to the line of sight than the others display anomalously large values of R.

In X-ray synchrotron jets, R is often a sharply decreasing function of distance down the jet ("class 1" e.g. 3C273, Jester et al. 2006), and we normally ascribe this to a decreasing ability to produce electrons of the required energies (possibly caused by an increasing magnetic field strength). In other straight jets normally thought to be representative of IC/CMB X-ray emission, the ratio may decrease smoothly (mimicking the synchrotron) or is sensibly constant down the jet ("class 2" e.g. 4C19.44, Schwartz et al. 2007). Normally these two possibilities are ascribed to a smoothly decelerating flow (thereby diminishing the IC component) or a relatively uniform value for Γ which would maintain the effective energy density of the CMB.

For a curved jet with changing θ , there may be anomalous changes in synchrotron brightness associated with the effect of θ on δ (the beaming factor), but the ratio of X-ray to radio emission should be preserved and remain unaffected by changing θ . In the IC/CMB scenario, the critical point is that a smaller θ will lead to a marked change in R (unlike the synchrotron case), deviating either from the smoothly decreasing ratio or from a constant ratio.

The knot S11.3 is brighter than adjacent knots in all 3 bands (radio, optical, and X-rays). Is this because it is where the curving jet lies closest to the l.o.s. or is it just an intrinsically stronger emitting region which might be caused by a longer path length at a tangential point? The longer pathlength possibility will again not disturb the intrinsic X-ray/radio behavior for either emission mechanism, so if we can show that S11.3 has an anomalously large ratio, it will be a strong indicator that the X-ray emission process is IC/CMB.

For IC/CMB emission, the preference for IC scattering when the electrons are meeting the photons 'head-on' in the jet frame, produces more IC emission in the downstream direction. The angular dependency of this extra beaming term is given in eq. (A22) of Harris & Krawczynski (2002) and with a few substitutions can be written as:

$$\xi = \left\{ 1 + \frac{\mu\Gamma - \sqrt{\Gamma^2 - 1}}{\Gamma - \mu\sqrt{\Gamma^2 - 1}} \right\}^2 \quad (1)$$

where Γ is the bulk Lorentz factor of the emitting region and $\mu = \cos\theta$. This function is shown in fig. 6 for a few representative values of Γ .

Although our data for 3C 17 are inadequate to perform a meaningful test, current parameters are given in Table 5 as an illustration of the method. While it is true that R is larger for S11.3 than for the adjoining knots, R(S3.7) is more than twice R(S11.3). To sustain an IC/CMB explanation for the X-rays of both knots, it becomes necessary to posit a smaller value of Γ for the outer parts of the jet compared to that ascribed to S3.7. That would mean that the Γ^2 term in eq.(A22) (*ibid*) would dominate the change in R between S3.7 and S11.3. In the present context the beaming parameters for S3.7 could be (see § 3) $\Gamma = \delta=8$, $\theta=7^\circ$ while at S11.3, $\Gamma=5.4$, $\delta=5.4$, and $\theta=10^\circ$ and in this case, the angular dependence is not the dominant effect. Obviously we have too much freedom because of the short *Chandra* observation:

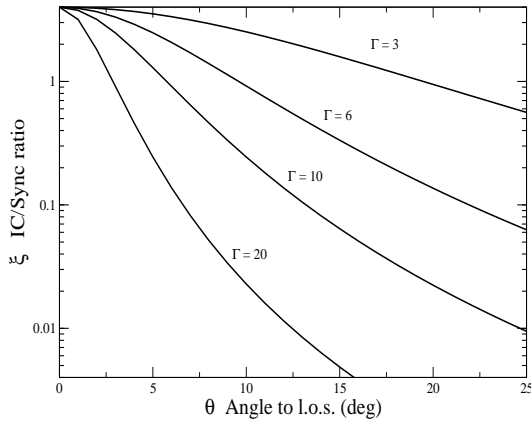


FIG. 6.— The function ξ describing the effects of the extra beaming factor on the ratio of IC/CMB to synchrotron emission. Curves for four representative values of Γ (3, 6, 10, and 20; top to bottom) are shown.

TABLE 5
X-RAY TO RADIO FLUX RATIO FOR THE JET OF 3C 17

Knot	$\nu * S_{5GHz}$ (10^{-15} cgs)	X-ray Flux (10^{-15} cgs)	Ratio
S3.7	1.45	6.4	4.4
S10.3	1.06	< 1.6	< 1.5
S11.3	3.83	7.1	1.9
S10.8	3.24	1.6	0.5
S9.6	1.80	< 1.6	< 0.9
S8.0	1.25	< 1.6	< 1.3
S7.2	4.63	< 1.6	< 0.3

Notes to table

The X-ray flux is for the band 0.5 to 7 keV from our 8ks observation. Dividing col.3 by col.2 yields the ratios of column 4. The X-ray flux of S10.8 comes from a single event and is reported here for illustrative purpose only

what is required for this test is a longer observation which would provide robust X-ray detections of all the knots in Table 5 so as to compare R values all along the jet.

Other sources with curved jets are 3C120 (for which it is not obvious where θ is at a minimum) and 4C65.15,

a higher redshift quasar whose morphology mimics that of 3C 17 and also has an X-ray detection of a knot at the location of maximum curvature of the jet (Miller & Brandt 2008).

5. SUMMARY

We have detected two knots in the 3C 17 jet in both X-rays and optical/IR bands. The resulting radio to X-ray spectra do not provide a definitive answer to the choice between IC/CMB and synchrotron X-ray emission. Additionally, we have described a peculiar optical object, possibly an edge-on spiral galaxy, which appears to be pierced by the jet. Although our X-ray data are not sufficient for the detection of additional jet knots, we have shown how the ratio of X-ray to radio intensities for the knots of curved jets can be used as a diagnostic for the X-ray emission process. IC/CMB emission, being more tightly beamed than synchrotron emission would be manifest by a larger ratio for a knot moving closer to the line of sight than its neighbors.

We thank the anonymous referee for useful comments that led to improvements in the paper. We thank R. Morganti for giving us her 5 GHz VLA map of 3C 17. F. Massaro is grateful to G. Migliori and S. Bianchi for their suggestions in the *Chandra* data analysis, A. Siemiginowska for her help in the use of the *Chandra* CIAO data reduction analysis software, and E. Liuzzo and S. Giacintucci for their suggestions about the radio data analysis. This research has made use of NASA's Astrophysics Data System; SAOImage DS9, developed by the Smithsonian Astrophysical Observatory; and the NASA/IPAC Extragalactic Database (NED) which is operated by the Jet Propulsion Laboratory, California Institute of Technology, under contract with the National Aeronautics and Space Administration. The National Radio Astronomy Observatory is operated by Associated Universities, Inc., under contract with the National Science Foundation. The work at SAO is supported by NASA-GRANT GO8-9114A.

Facilities: VLA, HST, CXO (ACIS)

REFERENCES

- Cardelli, J. A., Clayton, G. C., Mathis, J. S. 1989, *ApJ*, 345, 245
 Buttiglione, S., Capetti, A., Celotti, A., Axon, D.J., Chiaberge, M., Macchetto, F.D., Sparks, W.B. 2008, *A&A*, submitted
 Dickson, R., D. 1997, PhD thesis, Univ. Sheffield
 Donzelli, C. J., Chiaberge, M., Macchetto, F. D. 2007, *ApJ*, 667, 780
 Harris, D. E., Krawczynski, H. 2002, *ApJ*, 565, 244
 Harris, D. E., Krawczynski, H. 2006, *ARA&A*, 44, 463
 Jester, S., Harris, D. E., Marshall, H. L., Meisenheimer, K. 2006, *ApJ*, 648, 900
 Kalberla, P.M.W., Burton, W.B., Hartmann, D. 2005, *A&A*, 440, 775
 Ledlow, M. J., Owen, F. N. 1996, *IAUS*, 175, 238L
 Miller, B. & Brandt, N., 2008 *ApJ*, submitted
 Morganti, R., Killeen, N. E. B., Tadhunter, C. N., 1993 *MNRAS*, 263, 1023
 Morganti, R., Oosterloo, T., Tadhunter, C. N. 1999 *A&AS*, 140, 355
 Protheroe, R. J., 2004 *Aph*, 21, 415
 Schmidt, M. 1965 *ApJ*, 141, 1
 Schombert, J. M., Pildis, R. A., Eder, J. A., & Oemler, A., 1995, *AJ* 110, 2067
 Schwartz, D. A., et al. 2007, *Ap&SS*, 311, 341
 Siebert, J., Brinkmann, W., Morganti, R. 1996, *MNRAS*, 279, 1331
 Spergel, D. N., et al. 2007, *ApJS*, 170, 377
 Tadhunter, C. N., et al., 1998, *MNRAS*, 298, 1035
 Tavecchio, F., Maraschi, L., Sambruna, R. M. 2000 *ApJ*, 544L, 23
 Venturi, T., Morganti, R., Tzioumis, T., Reynolds, J. 2000, *A&A*, 363, 84